JTUSCI

Available online at www.taibahu.edu.sa

ISSN: 1658-3655

Bourja et.al. / JTUSCI 4: 1-8 (2010)

Taibah University for Science Journal

Inorganic Chemistry

Synthesis and characterization of nanosized $Ce_{1-x}bi_xo_{2-\delta}$ solid solutions for catalytic applications

L. Bourja[1, 2], B. Bakiz[1, 2], A. Benlhachemi[1*], M. Ezahri[1], S. Villain[2], J.R.Gavarri[2]

[1] Laboratoire Matériaux et Environnement LME, Faculté des Sciences, Université Ibn Zohr, BP 8106, Cité Dakhla, Agadir, Maroc ; [2] Institut Matériaux Microélectronique et Nanosciences de Provence, IM2NP, UMR CNRS 6242, Université du Sud Toulon-Var, BP 20132, 83957, La Garde Cedex, France

Received May 19th 2009; revised February 17th 2010; accepted February 21st 2010

Abstract

This study consists of elaborating and characterizing some nanometric materials in basic of rare-earth oxides by the soft chemistry technique. the first step of this work consists of synthesizing nanometric pure ceria by sol-gel process. In the second one, the Bismuth doped ceria by co-precipitation method was realized in order to obtain ceria-based solid solution, to improve its catalytic property by creation of oxygen vacancies. The solubility limit of Bi_2O_3 in CeO_2 was determined to be around 20 atom %. The effect of thermal treatment temperatures on the average crystallite sizes and lattice parameters was done for pure ceria and $Ce_{1-x}Bi_xO_{2-x/2}$ (x = 0.15 and 0.2). The different elaborated samples are subject of structural characterization (XRD). Catalytic reactivity of these materials in presence of "air- toxic gas" mixtures is studied by Fourier Transform Infra-Red Spectroscopy (FTIR).

Keywords: Catalytic properties; cerium bismuth oxide; $Ce_{1-x}Bi_xO_{2-\delta}$; soft chemistry; XRD.

Corresponding author: a.benlhachemi@gmail.com

1. Introduction

Pure and doped cerium oxides (ceria) are actual up-to-date materials for many industrial applications: gas sensors, solid electrolytes in solid oxide fuel cells (SOFC), ceramic, pigments and industry of catalysts. Indeed, ceria is used in three-way catalytic (TWC) for removing hydrocarbons C_xH_y, carbon monoxide CO and azote oxide NO_x from automobile exhausts due to its low redox potential between Ce^{3+} and Ce^{4+} and its high mobility of oxygen defects. This considerable diversity of ceria applications is strongly linked to its single properties such as: interesting physical-chemical ceria properties, its ability to catalyse at the same time reactions of oxidation and those of reduction and its nonstoichiometric behaviour. Ceria have a fluorite structure with space group F_{m3m} in which each cerium site is surrounded by eight oxygen sites in FCC arrangement and each oxygen site has a tetrahedron cerium site.

The goal of the present work was to prepare $Ce_{1-x}Bi_xO_{2-\delta}$ solid solutions ($0 \leq x \leq 1$). The influence of composition and calcination temperatures is discussed. The choice of Bismuth was based on this valency (+III) inferior to cerium's (+IV) one in ceria in the most stable state, which allow improving catalytic property of the ceria.

2. Experimental procedure

Nanosized powder of pure ceria was first synthesized via sol-gel method using nano-hydrate cerium (+III) oxalate ($Ce_2(C_2O_4)_3.9H_2O$, purity 99.9 %) mixed in absolute ethanol.

Samples of Bismuth doped ceria $Ce_{1-x}Bi_xO_{2-x/2}$ ($0 \leq x \leq 1$), were produced with co-precipitation method using the appropriate quantities of cerium (+III) nitrate hexahydrate ($Ce(NO_3)_3.6H_2O$, purity $\geq$ 98 %) and Bismuth (+III) nitrate pentahydrate ($Bi(NO_3)_3.5H_2O$, purity $\geq$ 98 %) which were dissolved separately in a suitable volume of distilled water. Both nitrate solutions were mixed and stirred for two hours at room temperature. Ammoniac (NH_4OH) was added to the mixture in order to adjust pH (pH = 10). The obtained precipitate was filtered, washed with distilled water in order to remove residual NH_4^+ and dried at 80°C. Finally, the precursor powder was calcined for 6 hours at 600 °C.

3. Results & discussion

The polycrystalline samples were analyzed by X-ray diffraction, using a D5000 Siemens - Bruker diffractometer, equipped with a copper X-ray source (wavelength λ = 1.54 x 10^{-10} m ; tension V=45 kV, intensity I=35 mA), and with a monochromator eliminating K_β radiation. Analysis were carried out using the classical θ-2θ configuration, with 2θ angle steps of 0.02° and counting times of 19 s per step. The average crystallite's size of the prepared powders was evaluated from the half-widths of diffraction peaks using the Scherrer formula [i]:

$$D = \frac{K.\lambda}{\beta.\cos(\theta)}$$

where λ is the wavelength of X-ray ($\lambda_{CuK\alpha1}$= 1.54 x 10^{-10} m) ; K is a Scherrer constant (K = 0.9 in this case) ; θ is the diffraction angle associated with a Bragg peak; $\beta=(\beta_m^2-\beta_s^2)^{1/2}$ is the corrected full width at half maximum (FWHM), β_m being the total FWHM of the Bragg peak, β_s being that of a standard crystallized sample of CeO_2. The Lattice parameters of compounds were calculated and refined by PARAM program using least squares method. Analysis of the obtained spectra is done by WinPlotr program.

3.1 Characterization of pure ceria

Figure 1 shows the obtained diffractogrammes of pure ceria samples calcined at different temperatures.

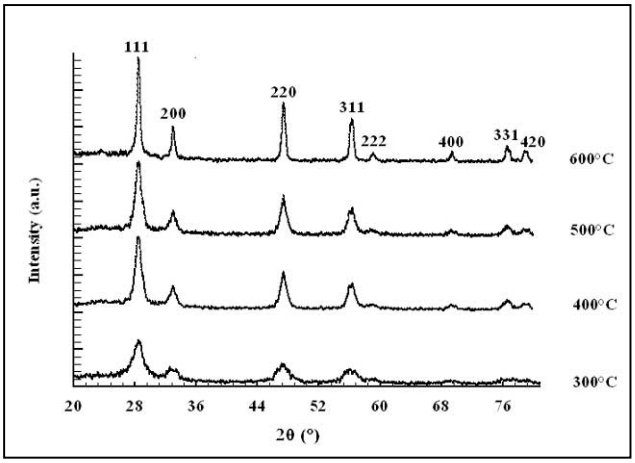

Fig. 1. X-Ray Diffraction patterns of pure ceria samples obtained at different calcination temperatures.

X-ray diffraction patterns revealed that all peaks are indexed in CeO_2 fluorite structure (JCPDS: 34-0394). The XRD peaks became gradually sharper with increasing temperature and the average crystallite size increased from 5 to11 nm for temperatures of 300 and 600 °C respectively, indicating that the crystallinity of CeO_2 is accelerated by calcination process. In Table 1, the lattice parameter a and the crystallite size D calculated by Scherrer formula were reported. Figure 2 illustrates the relationship between the calcination temperature and the average crystal size of CeO_2 nanoparticles. It can be seen that the crystallite size increases with increasing calcination temperature and becomes especially more large in the range of 500-600 °C. Generally, it can be considered that the CeO_2 nanocrystallites grow mainly by means of interfacial reactions. The lattice parameter decreases from 0.5406 to 0.5403 nm with increasing calcination temperature (Table 1). This result may be explained by the increasing of the densification of our samples.

3.2 Characterization of Bismuth doped ceria

3.2.1 Structural study

X-ray diffraction shows that a strong variation occurs in the phase system as bismuth atom fraction increases. Figure 3 (a, b, c and d) shows the X-ray diffraction patterns for samples noted (1-x) CeO_2 , $x/2Bi_2O_3$ with x varying between 0 and 1. The results of XRD analysis indicate that for the compositions $0 \leq x \leq 0.20$ a single phase is observed with a cubic fluorite structure as pure ceria (JCPDS : 34-0394; Fig. 3a). No Bismuth oxide phases were detected by XRD. This may be due to the formation of Bi/Ce oxide solid solution with fluorite structure. Above composition of x=0.20, a multiphase system is evidenced and the ceria based phase presents a constant cell parameter a = 0.5421 nm: the two new additional phases are identified as being tetragonal and closely related to bismuth oxide structural varieties. Their cell parameters were refined. In the composition range 0.3 to 0.7 (Fig. 3b), a tetragonal β' phase is observed with refined cell parameters: a = 15.542 ± 0.003 Å; c = 5.645 ± 0.001 Å. It is a superstructure of the tetragonal β phase observed for compositions 0.8 and 0.9 (Fig. 3c), with refined cell parameters: a = 7.742 ± 0.001 Å; c = 5.633 ± 0.001 Å. The observed pure Bi_2O_3 phase is monoclinic (Fig. 3d). These substituted phases were never observed, and testing structural models are in improvement in order to describe these phases.

Table 1. Lattice parameter (a), and crystallite size (D) of CeO_2 calculated by Scherre formula ± standard deviation.

Temperature (°C)	Lattice parameter a(nm)	Crystallite sizes D(nm)
300	0.5406 ± 0.0002	5.92 ± 0.05
400	0.5405 ± 0.0003	6.14 ± 0.05
500	0.5404 ± 0.0001	6.68 ± 0.06
600	0.5403 ± 0.0001	11.2 ± 0.2

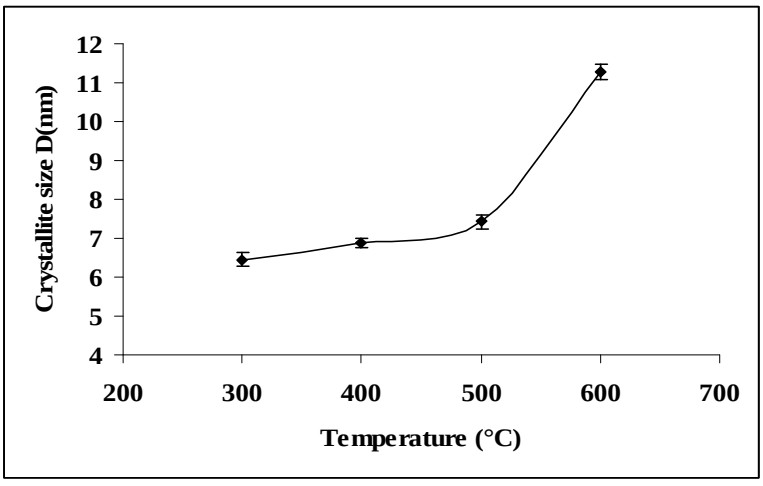

Fig. 2. Effect of calcination temperature on the crystallite sizes of CeO_2 nanoparticles.

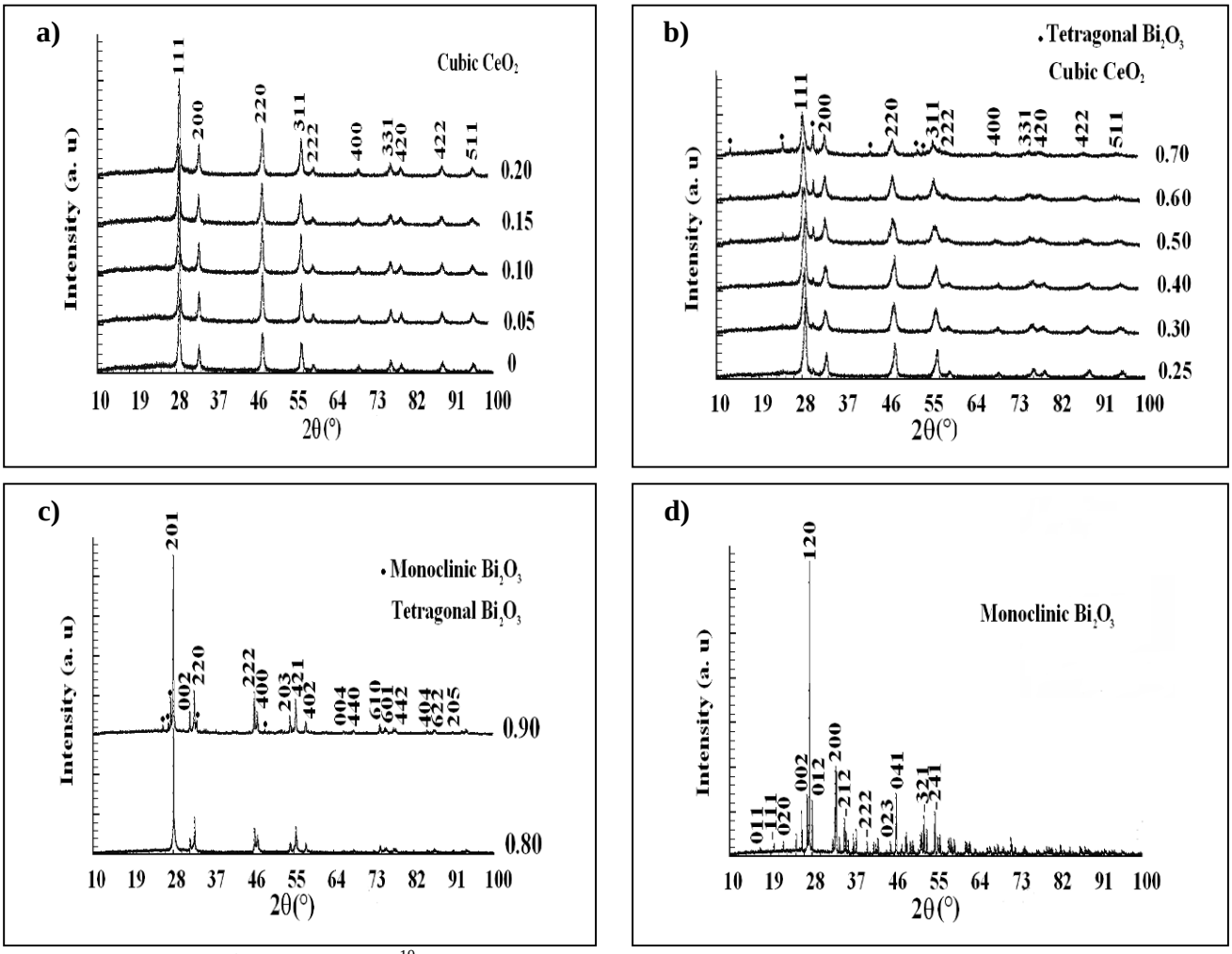

Fig. 3. XRD patterns ($\lambda_{CuK\alpha1}$= 1.54 .10^{-10} m) of samples [(1-x)CeO_2 ; x/2Bi_2O_3] heated at 600°C. (a): XRD patterns for $0 \leq x \leq 0.20$; (b): XRD patterns for $0.25 \leq x \leq 0.70$ biphasic system; (c): x=0.8 and 0.9 ; (d): x=1 (α-Bi_2O_3).

The unit cell parameter increases with increasing Bi content (Fig. 4) up to 20% Bi and then remains constant with further Bi additions. Such an increase in the lattice constant is considered to be due to the substitution of Ce^{4+} ions (r_{Ce4+} = 0.097 nm) with larger Bi^{3+} ions (r_{Bi3+} = 0.117 nm). The substitution reaction can be described by taking into account the Kröger-Vink notation by the following equation [15]:

$$Bi_2O_3 \longrightarrow 2Bi'_{Ce} + Vo^{\cdot\cdot} + 3O_o$$

where (Bi'_{Ce}) defects of Ce^{3+} ion that present negative charge compared with Ce^{4+} which will be substituted by Bi^{3+},($Vo^{\cdot\cdot}$) designates an oxygen vacancy, (Oo) = O^{2-} ion on a regular oxygen lattice site. From this equation the formation of oxygen vacancies because of charge compensation should be assumed [16].

The linear variation of the lattice parameter as a function of Bismuth content x (Fig. 4) can be expressed by: a (nm) = 0.0059 xs + 0.541. It is suggested that the solubility limit of Bi^{3+} in CeO_2 is around 20 atom %. The same results were obtained by Dikmen but with a hydrothermal reaction [13].

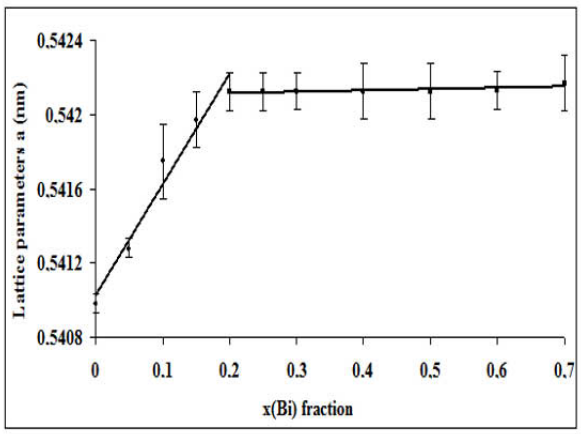

Fig. 4. Variation of cubic cell parameter a as a function of x.

The average crystallite size D of Bismuth substituted ceria powders calculated using the Scherrer formula decreased with rate of Bi doping (Fig. 5). This result confirms that crystallite size depends on solid solution composition and the substitution of Ce^{4+} by Bi^{3+} enable to obtain smaller crystallites which is interesting for the catalyses.

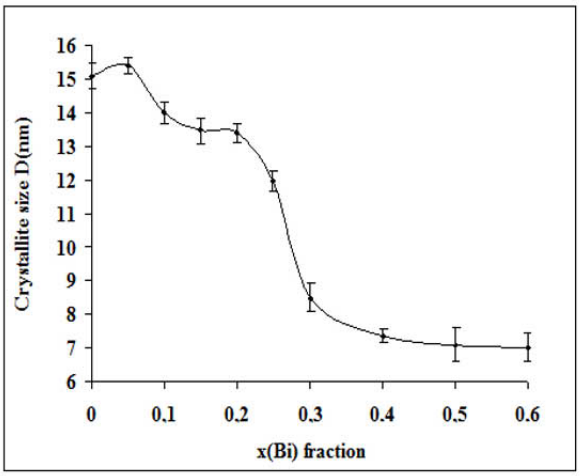

Fig. 5. Variation of cubic crystallite size D as a function of x .

3.2.2 Effect of the calcination temperature

It is known that the thermal treatments influence powders granulometry and their catalytic properties. Indeed, the average crystallite's size increases with calcination temperature which leads to the decrease of specific surface and the catalytic activity.

In order to follow the variation of crystallization Bi doped ceria prepared by co-precipitation synthesis, a study of XRD as a function of temperature was realized for two samples (x = 0.15 and x = 0.2). The obtained diagrams are represented on Figures 6 and 7. For composition x = 0.15 of Bismuth, all of XRD patterns shows that only diffraction peaks of pure ceria (JCPDS: 34-0394) exist. Composition x = 0.2 of Bismuth and for T ≥ 1000 °C Bi_2O_3 monoclinic structure (JCPDS: 41-1449) appears in addition to ceria phase. I addition, the comparison of X-rays diffraction patterns for the two samples shows that FWHM of the Bragg peaks decrease with increasing calcination temperatures. This is due to growth crystallite size.

The variation of the lattice parameter according of the temperature presents the same appearance for the two samples (Fig. 8). However, a difference exists of the maximum temperature (800°C and 900°C for composition 0.15 and 0.2 respectively). The increase of the lattice parameter may be explained by reduction of Ce^{4+} to Ce^{3+} with large radius (r_{Ce3+}= 0.128nm) which is issue from the deficiency of oxygen.

The average crystallite sizes of $Ce_{0.85}$ $Bi_{0.15}$ $O_{2-\delta}$ and $Ce_{0.8}$ $Bi_{0.2}$ $O_{2-\delta}$ calculated by Scherrer formula increased with calcination temperature (Fig. 9). This variation of the grain size may be explained by the sintering theory.

3.2.3 Catalytic study

The Bi_2O_3-CeO_2 materials were exposed to air-CH_4 and air-CO gas flows in a homemade cell, and the conversion into CO_2 was analyzed by Fourier transform infrared (FTIR) spectroscopy, using a FTIR Unicam-Mattson spectrometer working with cube corner technology. The gases pass through a polycrystalline porous wall constituted of the various phases. Figure 10 shows the experimental setup. The catalytic reactor is a cylindrical cell in which the sample can be exposed to reactive air-gas flow. The sample temperature is controlled by a thermocouple and stabilized at a given T_{react} value corresponding to a given reactivity. A fixed mass (m_0 = 0.1 g for each test) of powder is placed between two porous (ZrO_2) separators. Blank experiments with these separators were systematically carried out to confirm the absence of activity in the cell itself. The gas flow, controlled by flow meter (2500 ppm CO in air or CH_4 in air), passed through separator 1, then the sample, and finally separator 2, with a fixed slow speed (10 sccm). The reactor is heated in a furnace, at temperatures ranging between 100°C and 525°C.

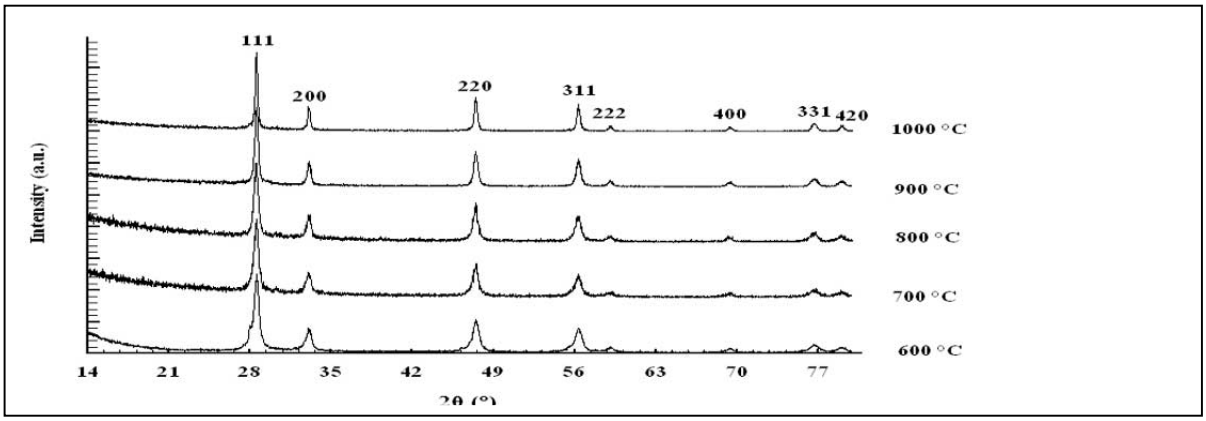

Fig. 6. Variation of XRD patterns of $Ce_{0.85}Bi_{0.15}O_{2-\delta}$ as a function of thermal treatment temperatures.

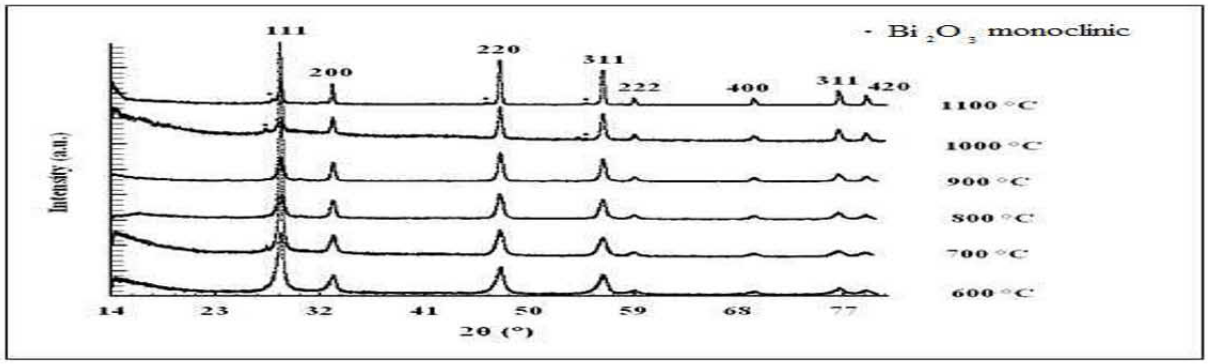

Fig. 7. Variation of XRD patterns of the $Ce_{0.8}$ $Bi_{0.2}O_{2-\delta}$ as a function of thermal treatment temperatures**.**

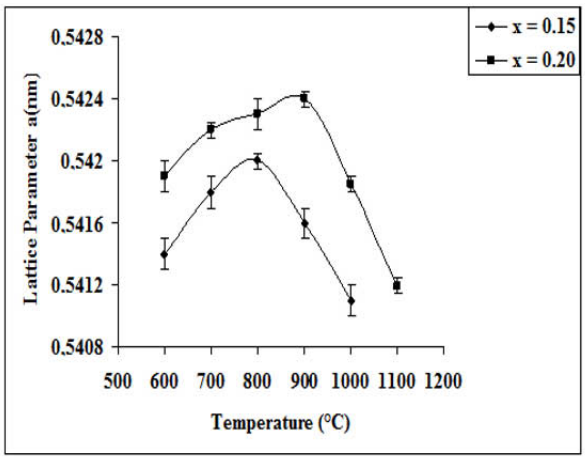

Fig. 8. Variation of lattice parameter bismuth doped ceria according to the calcination temperature.

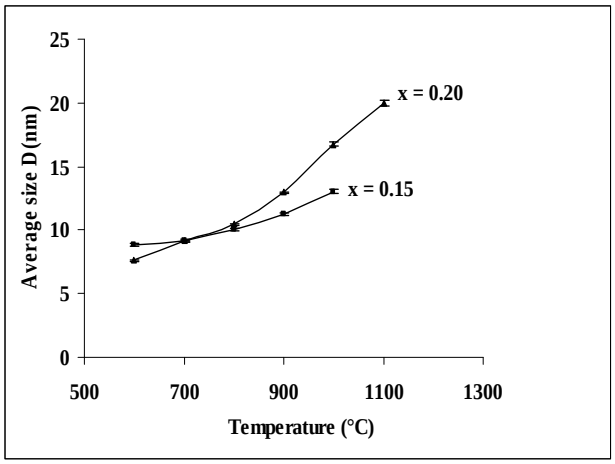

Fig. 9. Variation of crystallite average size of the bismuth doped ceria according to the calcination temperature.

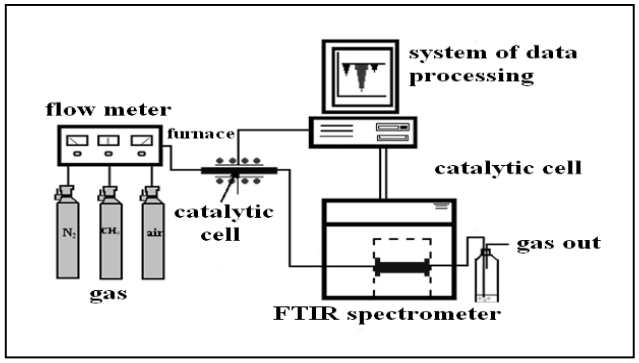

Fig.10. Homemade catalytic device (gas feed, furnace, FTIR analysis)

The catalytic response of nanometric powder of pure ceria, $Ce_{0.80}Bi_{0.20}O_{2-\delta}$ and bismuth oxide with air-CH_4 and air-CO flows at two temperatures (250°C and 500°C) was presented on Figures 12 and 13. The conversion reactions are revealed by the appearance of the infrared absorption band of CO_2 (doublet at 2340 - 2360 cm^{-1}), resulting from oxidation of CH_4 and CO. The emitted gases were then analyzed by Fourier Transform Infrared (FTIR) spectroscopy.

On one hand for CH_4, the intensity of CO_2 peak decreases according to the composition of the Bi, which means that the samples rich of Bi aren't a good catalyst for CH_4. On the other hand for CO, we observe an increase of the same peak's intensity. So we conclude that these materials (i.e. samples rich of Bi) can be used as a catalyst of the CO oxidation reaction.

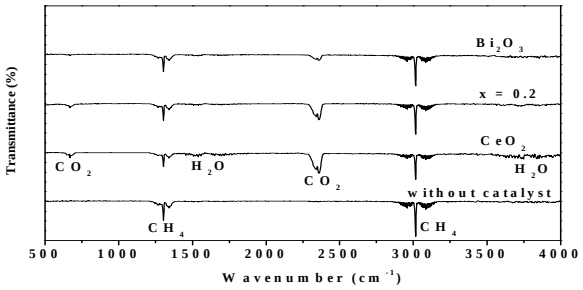

Fig.11. Spectre FTIR of gas obtained after catalytic effect at 500°C with air-CH_4

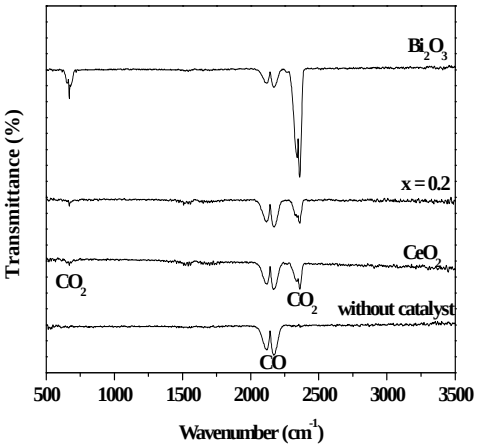

Fig.12. FTIR spectra of gas after catalytic effect at 250°C with air-CO

Conclusion

A series of ceramic samples belonging to the CeO_2-Bi_2O_3 phase system have been prepared via a co-precipitation route. The crystallized phases were obtained by heating the solid precursors at 600°C for 6 hours, then quenching to room temperature. X-ray diffraction analysis shows that for $x \leq 0.20$ a solid solution $Ce_{1-x}Bi_xO_{2-x/2}$ with fluorite structure is formed. For x ranging between 0.25 and 0.7, a tetragonal β' phase coexisting with the FCC solid solution is observed. For x ranging between 0.8 and 0.9, a new tetragonal β phase appears. The β' phase is postulated to be a superstructure of the β phase. Finally, close to x=1, the classical monoclinic α-Bi_2O_3 structure is observed.

Next, the unit cell parameter increases with increasing Bi content which is in good agreement with effective ionic radii considerations (r_{Bi3+} = 0.117 nm, r_{Ce4+} = 0.097 nm). The linearly variation of lattice parameter as a function of doping rate obeys the Vegard's low. The solubility limit of Bi^{3+} in CeO_2 is around 20 atm %. The average crystallite size decreases with rate of Bi doping element. This confirms that crystallite size depend on solid solution composition and the substitution of Ce^{4+} by Bi^{3+} enables to obtain smaller crystallites.

On the other hand, the catalytic tests show that samples rich of Bismuth are a good catalyst for CO oxidation reaction.

References

[1]A. Trovarelli (1996). Catalysis Reviews: Science and Engineering. 38: 439–520.

[2]A. Tschope, W. Liu, M. Flytzani-Stephanopoulos, and J. Y. Ying, (1995) Journal of Catalysis.157: 42–50.

[3]M. Mogensen, N. M. Sammes, and G. A. Tompsett, (2000). Solid State Ionics. 129: 63–94.

[4]M. Kamruddin, P. K. Ajikumar, R. Nithya, A. K. Tyagi, Raj Baldev (2004). Scripta Materialia. 50: 417-422.
[5]K. Ouzaouit, A. Benlhachemi, L. Aneflous, H. Benyaich, J. R. Gavarri, J. Musso (2005). Journal Phys. IV France. 123: 125-130.
[6]A. A. Bukaemskiy, D. Barrier, G. Modolo (2006). Journal of the European Ceramic Society. 26: 1507-1515.
[7]Y. Ikuma, K. Takao, M. Kamiya, E. Shimida (2003). Materials Science and Engineering B99: 48-51.
[8] N. G. Millot (1998). Thèse de l'Université de Borgonge.
[9]J. F. Berrar (2000). Ecole centrale PARIS, 92295 Châtenay-Malabray private commutations.
[10]J. R. Carvajal, T Roisnel, Winplotr (2005) a Graphic Tool for powder diffraction.
[11]H. Yang, C. Huang, A. Tang, X. Zhang, W. Yang. (2005). Materials Research Bulletin. 40: 1690-1695.
[12]J. L. M. Rupp, C. Solenthater, P. Passer, U. P. Muecke, L. J. Gauckler (2007). Acta Materialia. 55: 3505-3512.
[13]S. Dikmen, P. Shuk, M. Greenblatt(1998). Solid State Ionics. 112: 299-307.
[14]L. Bourja, B. Bakiz, A. Benlhachemi, M. Ezahri, J.C. Valmalette, S. Villain, J.R.Gavarri, (2009). Advances in Materials Science and Engineering, Volume 2009, Article ID 502437, 4 pages doi:10.1155/2009/502437.
[15]V. Gil, C. Tours, P. Duran, J. Tartaj (2007). Solid State Ionics. 178: 359-365.
[16] V. Gil, J. Tartaj, C. Moure, P. Duran (2007). Journal of the European Ceramic Society. 27: 801-805.
[17]R. D. Shannon (1976). Acta Crystallogr, A 32: 751-767.
[18]P. Nowakski S. Villain, A. Kopia, I. Suliga J.R. Gavarri, (2008). Applied Surface Science. 254: .5675-5682.